atmosphere

MDPI

Article

A Study on Avalanche-Triggering Factors and Activity Characteristics in Aerxiangou, West Tianshan Mountains, China

Jie Liu [1,2,†], Tianyi Zhang [1,2,*,†], Changtao Hu [2,*], Bin Wang [2], Zhiwei Yang [2], Xiliang Sun [1,2] and Senmu Yao [2,3]

[1] School of Transportation and Logistics Engineering, Xinjiang Agricultural University, Urumqi 830052, China; hfutliujie@163.com (J.L.); 320222586@xjau.edu.cn (X.S.)
[2] Xinjiang Transport Planning Survey and Design Institute Co., Ltd., Urumqi 830006, China; wangbin13245@126.com (B.W.); yangzhiwei19@mails.ucas.ac.cn (Z.Y.); 107552204581@stu.xju.edu.cn (S.Y.)
[3] College of Civil Engineering and Architecture, Xinjiang University, Urumqi 830046, China
* Correspondence: zhangtianyikevin@outlook.com (T.Z.); xj11992023@163.com (C.H.)
† These authors contributed equally to this work.

Abstract: Through analyzing the triggering factors and activity characteristics of avalanches in Aerxiangou in the Western Tianshan Mountains, the formation and disaster-causing process of avalanches were studied to provide theoretical support and a scientific basis for avalanche disaster prevention. In this paper, based on remote sensing interpretation and field investigation, a spatial distribution map of avalanches was established, and the induced and triggering factors in disaster-prone environments were analyzed using the certainty factor model. The degree of influence (E) of the disaster-causing factors on avalanche triggering was quantified, and the main control conditions conducive to avalanche occurrence in different periods were obtained. The RAMMS-avalanche model was used to analyze the activity characteristics at points where multiple avalanches occurred. Research results: (1) The E values of the average temperature, average snowfall, and surface roughness in February were significantly higher than those of other hazard-causing factors, reaching 1.83 and 1.71, respectively, indicating strong control. The E values of the surface cutting degree, average temperature, and average snow depth in March were all higher than 1.8, indicating that these control factors were more prominent than the other factors. In contrast, there were four hazard-causing factors with E values higher than 1.5 in April: the mean temperature, slope, surface roughness, and mean wind speed, with clear control. (2) Under the influence of the different hazard-causing factors, the types of avalanches from February–April mainly included new full-layer avalanches, surface avalanches, and full-layer wet avalanches. (3) In the RAMMS-avalanche simulation test, considering the deposition effect, compared to the previous avalanche movement path, the secondary avalanche flow accumulation area impact range changes were slight, while the movement area within the avalanche path changes was large, as were the different categories of avalanches and their different movement characteristic values. Overall, wet snow avalanches are more hazardous, and the impact force is larger. The new snow avalanches start in a short period, the sliding rate is fast, and the avalanche sliding surface (full-snow surface and face-snow) of the difference is mainly manifested in the differences in the value of the flow height.

Keywords: avalanche; triggering factors; certainty factor model; activity characteristics; RAMMS

Citation: Liu, J.; Zhang, T.; Hu, C.; Wang, B.; Yang, Z.; Sun, X.; Yao, S. A Study on Avalanche-Triggering Factors and Activity Characteristics in Aerxiangou, West Tianshan Mountains, China. *Atmosphere* **2023**, *14*, 1439. https://doi.org/10.3390/atmos14091439

Academic Editor: Tin Lukić

Received: 9 August 2023
Revised: 6 September 2023
Accepted: 10 September 2023
Published: 15 September 2023

1. Introduction

An avalanche is a natural phenomenon widely occurring in mountains at middle and high latitudes, exhibiting seasonal, sudden, potential, and unpredictable characteristics [1–4]. The western Tianshan Mountains of Xinjiang, China, are limited by tectonic belts, which are conducive to the invasion of westerly airflows, thereby generating abundant precipitation. These typically folded fault block mountains widely contain ancient cirques and snow depressions, while a large amount of snow can accumulate in these mountains,

becoming the source of avalanches [5–7]. With the continuous development of transportation and tourism in mountain areas, avalanches have become one of the main natural disasters hindering development [8]. In March 2008, an avalanche induced by strong winds destroyed construction camps and buried construction tunnels in the Guozigou region of the Ili Kazakh Autonomous Prefecture in Xinjiang, resulting in the deaths of 16 people, injuries to 8 individuals, and the loss of the natural gas supply. In December 2010, an avalanche triggered by heavy snowfall impacted passing vehicles and cut off roads in the G218 Tianshan section, killing two people and trapping thousands of vehicles in the mountainous area. In April 2019, an avalanche buried a mountain road in Urumqi's Nanshan Scenic area, injuring and trapping 10 people [9]. Therefore, analyzing avalanche-triggering factors could facilitate the accurate control of regional main disaster factors, which has very important research value and practical significance for disaster prevention and reduction, disaster management, and decision-making.

The initiation of avalanches is closely related to the topography and geomorphology, snow characteristics, meteorological conditions, and human activities [5,10–12]. Among the above factors, the topography and landform as the basic conditions can trigger avalanches under the joint coupling and combination of snow characteristics, meteorology, human activities, etc. Many scholars have widely researched the triggering factors of avalanches. Schweizer et al. [10,13] stated that because the terrain is the only constant parameter during avalanche triggering, the slope in most avalanche formation zones ranges from 30~45°. Linke et al. [5], who studied the disaster mechanism of tabular avalanches, mentioned that the change in the shear force between the snowboard and the lower snow layer is the main cause of the rupture between snow layers and the triggering of avalanches. Schweizer, De Quervain [6,10,14], and others studied the relationship between wind-blown snow and avalanches, noting that wind-blown snow is more fragmented than naturally settled snow; hence, the snow layer formed by wind-blown snow is more susceptible to avalanches. Gratton et al. [15] found that the avalanche-triggering factors of the eastern slope and the western slope differ when considering the avalanche-triggering mechanism of slope direction. The avalanche triggering of the eastern slope depends on the accumulated snow amount of the slope area, while the western slope depends on occasional snowfall and temperature. At present, research on avalanche-triggering factors mostly focuses on the influences of individual factors on avalanche triggering, but rarely examines the influences of disaster factors on avalanches on small regional scales. In different disaster-prone environments, disaster-causing factors provide both advantages and disadvantages, leading to different triggering mechanisms.

Analyzing disaster-causing factors on a small scale is a prerequisite for improving the accuracy of regional disaster prediction. Since avalanche triggering is a complex nonlinear system, the degree of influence between causative factors varies among different regions and under different physical and geographic conditions. Therefore, mathematical models can be used to consider the relationship between the distribution of avalanches and causative factors and to analyze the dominant causative factors of avalanche triggering [16,17] to further elucidate avalanche-triggering factors within small-scale ranges and provide scientific references for avalanche disaster prevention and control.

At present, many scholars have used certainty factor (CF) models to study disaster-prone environments in the region and have achieved certain results. Mohsen Rezaei et al. [18] used the CF model and analytic hierarchy process (AHP) method to analyze the land subsidence sensitivity in the Neshapur Plain of Iran and found that the prediction accuracy of the CF model was much higher than that of the AHP method, which can be used to accurately distinguish areas with low, medium, high and very high susceptibility levels, thus providing high disaster prevention and control guidance value. Lin et al. [19] solved the problem of selecting and quantifying hazard factors in the process of landslide susceptibility evaluation by coupling the CF model and Stability INdex MAPping (SINMAP) model and applied this method in the Wulingshan area of Cili County, Hunan Province, which provided a new idea for regional rainfall-induced landslide forecasting.

Wang Zhiheng [16] found that the geotechnical type, elevation, and slope control the distribution of rainfall-type landslides in the study area using the CF model, and the results could be quantitatively analyzed to reflect the degree of influence of each disaster-inducing environmental factor on landslide destabilization. Based on the Google Earth Engine (GEE) cloud computing platform, Mao Zhengjun [20] selected eight influencing factors of terraced loess landslides and used the deterministic coefficient method to analyze these factors, revealing that the main control factors of their formation were rainfall and stratigraphic lithology. Xiang Lingzhi et al. [21] used the coefficient of certainty to analyze the environmental factors that can cause disasters in the Wenchuan earthquake disaster area and further determined the dominant factor interval affecting the occurrence of disasters in the area. The above research results indicate that the CF value can be considered to more objectively determine the main control factors of disaster triggering on a small regional scale. This method is simple and easy to apply and can be suitably employed to study the influences of disaster-causing factors. Therefore, the CF model can be utilized to explore the degree of influence of each causative factor in the avalanche-prone environment to reveal the causative mechanism of avalanches on a small scale.

Using high-resolution remote sensing image interpretation and field survey analysis, a spatial distribution map of avalanche disasters in Aerxiangou was established. Based on the CF model, the triggering factors in the avalanche-prone environment within the study area were analyzed, the main control factors were clarified, and the influence of disaster factors on avalanche triggering was quantified, thereby aiming to reveal the disaster mechanism in the avalanche area of Aerxiangou. The RAMMS-avalanche model was used to simulate and analyze the activity characteristics at typical avalanche points to determine the attributes of the avalanche motion trajectory and disaster formation process. The research results could provide theoretical support and a scientific basis for avalanche disaster prevention.

2. Data and Methods

2.1. Research Background

The Tianshan mountain range lies in a quasi-east-west direction. It has special topography and tectonics and is influenced by the west wind belt airflow. The West Tianshan Ili River Valley and the mountainous areas on both sides form a rich precipitation area. Its typical folds and fault-block mountains create an ancient ice bucket. Scattered snow erosion depressions can gather large amounts of snow, giving rise to the avalanches that occur in the area. The Aerxiangou, in the depths of the West Tianshan mountain area, is part of the middle- and high-altitude mountainous landscape. It lies along the latitudinal tectonic mountain range, comprising mountain basins and valleys, with gully valleys to both sides. The mountain is steep, with a general slope gradient of 40~60°, and has a high degree of undulation. Winter snows are of long duration; on individual windward slopes or slope sections, the snow depth can reach 100cm in snowy years. The southeast side of the forest has few avalanche traces. The northwest side of the mountain is bare and has low vegetation cover, a typical avalanche disaster breeding environment [18,19], as shown in Figure 1a,b.

In our investigation of Aerxiangou avalanche disasters from 2020~2023, it was found that there were multiple avalanche disaster points in the area. Avalanches caused damage to the infrastructure of the Y029 township, blocking traffic, wrapping the soil during the caving process, and causing serious soil loss.

During the period from 11 February to 20 April 2023, it was determined that there were 11 disaster points along the road within approximately 20 km of Aerxiangou, accounting for 12% of the total number of investigation points, with 81 hidden danger points. Among them, slope-based avalanches accounted for 16%, grooved avalanches accounted for 68%, and gully slope avalanches accounted for 15% of the total number. Fresh snow avalanches accounted for 59%, and wet snow avalanches accounted for 41% of the total number of avalanches. Past avalanches were mostly medium and small in scale, and avalanches were

mostly formed by slope instability, mainly fresh snow avalanches, as indicated in Table 1. The specific distribution of disaster points is shown in Figure 2c.

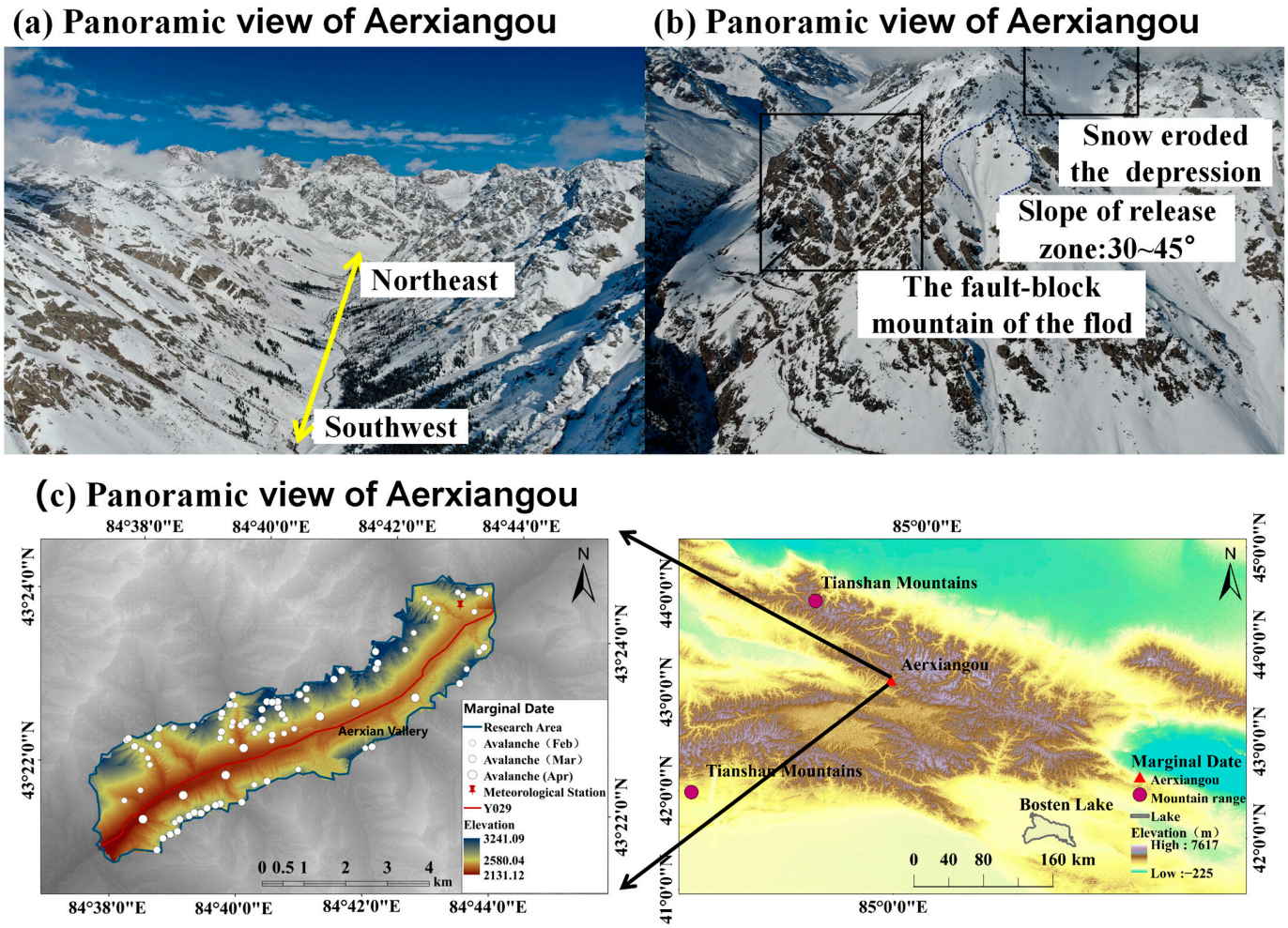

Figure 1. Topographic map of the study area.

Table 1. Statistics of the avalanche type.

Classification Basis	Avalanche Category	Quantity (Occurrence)	Proportion (%)
Total number of surveys	Disaster points	11	12%
	Hidden danger points	81	88%
Path morphology	Slope type	15	16%
	Groove type	63	68%
	Gully slope type	14	15%
Water content in snow	Fresh snow avalanche	54	59%
	Wet snow avalanche	38	41%
Pollution status of the accumulated debris at disaster sites	Clean stacks	6	54%
	Contaminated piles: trees, branches	2	18%
	Contaminated piles: Stones, clods	1	9%
	other	2	18%
Size of the stack (height of snow accumulation on the road surface)	>8; 5–8 m	0	0%
	3–5 m; 2–3 m	2	18%
	<2 m	5	45%
	Small avalanches and natural snowfall (1.2 m)	4	36%

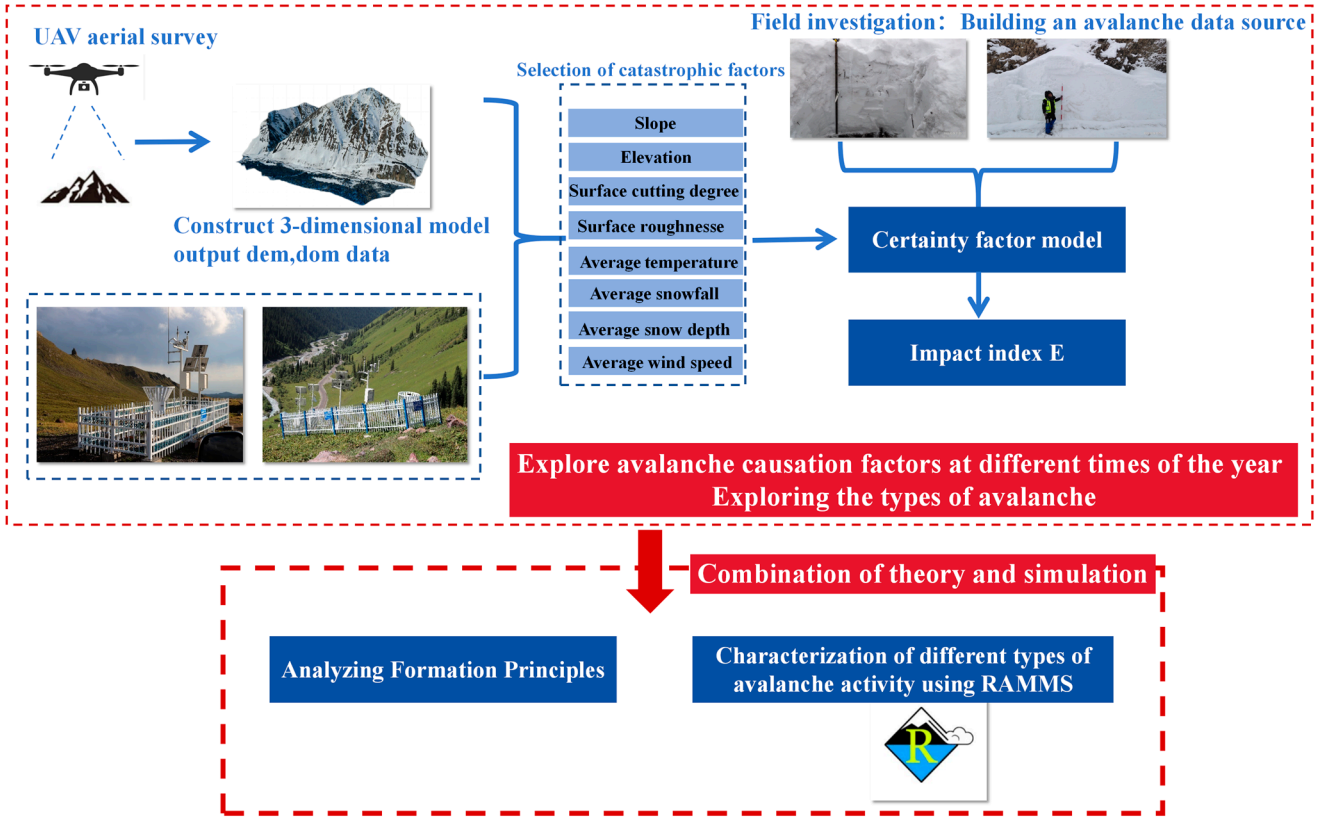

Figure 2. Technology roadmap.

2.2. Overall Procedure

To reveal the disaster-causing mechanism of the Arxiangou avalanche area, based on the establishment of the spatial distribution map of avalanche disasters in Arxiangou using the visual interpretation of high-resolution remote sensing images and the results of field investigations, the CF model was applied to analyze the inducing factors of an avalanche environment in the study area, to clarify the main controlling factors and to quantify the influence of the disaster-causing factors on the triggering of avalanches, and to analyze the activity characteristics simulation test of typical avalanche points to identify the trajectory of avalanche movement and the characteristics of the formation process. The avalanche simulation test analysis of typical avalanche points was used to identify the characteristics of avalanche trajectory and disaster formation process. Finally, the types of avalanches triggered by the primary and secondary controlling effects of the disaster-causing factors in different periods and their activity characteristics were clarified. Figure 2 shows the main workflow.

2.3. Data Sources

The data used in this study include a digital orthophoto map (DOM), a digital elevation model (DEM) dataset, and meteorological monitoring data. DOM and DEM data were obtained from DJI M300 RTK UAV aerial images recorded in February 2023 as the data source, and multi-view 3D modeling technology was used to process the recorded images and obtain DOM and DEM data. The geographical coordinates were based on the WG84 system, and the projection coordinates are based on the Gauss-Kruger approach. Regarding the temperature, wind direction, and air pressure, three observation indexes with high variability, the automatic weather station obtained sample data once every 1 s. The sampling method for wind speed occurred once every 0.25 s. Snow cover depth, solid precipitation, etc., were sampled once a minute. The specific meteorological monitoring equipment is shown in Figure 3.

Figure 3. Automatic weather station in Aerxiangou.

2.4. Selection of Hazard-Causing Factors

2.4.1. Selection of Topographic Factors

Topographic data are permanent parameters in avalanche prediction. Among them, slope is considered to be the main factor leading to avalanche instability, and slope can directly affect the stability of the snow layer by changing the force distribution of the snow layer and the thickness of the snowpack. According to statistics, avalanches are more likely to occur on slopes within a range of 25°~50°, and the frequency of avalanches increases when the slope gradient exceeds 36° [20,21]. Due to the prevalence of ice avalanche action above and below the mean snow line (3680 m) in the western Tianshan Mountains, small and medium avalanche hazards develop easily, while the elevation values can reflect the lineal height of the mountains and snow line in the study area [22]. Thus, the elevation and slope determine the magnitude and frequency of avalanches. Aerxiangou lies within a small-scale area, and avalanches tend to occur in short gullies and slopes. Therefore, to accurately measure the influence of the mountain morphology on avalanche triggering and to characterize the relative changes in the small-scale geomorphology, composite parameters, such as surface cutting degree and surface roughness, were considered to measure the regional avalanche stability. The higher the surface cutting degree, the greater the rate of vertical change in ground morphology, resulting in poor slope snow capacity; avalanche stability becomes weaker, while the level of ground roughness is a direct response to the magnitude of the sliding force between the snow layer and the subsurface. Quantifying the relative changes in regional landforms through such composite parameters is intended to reveal the relationship between landform morphology and snowpack, thereby revealing the relationship between the geomorphic morphology and snowpack features.

2.4.2. Meteorological Factor Selection

New snowfall (fresh snow), wind, and temperature are meteorological factors that significantly influence avalanche triggering [22,23]. Avalanches due to heavy snowfall occur more frequently in the western Tianshan Mountains, especially in early February [24]. A balance exists between the increase in the downslope stress caused by settling during snowfall and the increase in the strength of the snow body, with the former destabilizing the snow body and the latter increasing the stability of the snow layer. Thus, heavy snowfall is the most important causal factor of large catastrophic fresh snow avalanches [25]. Valley winds are second only to fresh snowfall as a meteorological factor influencing avalanches. Secondary transport by wind can cause snow to settle at a higher rate at some locations, while changes in wind speed can cause wind-blown snow to form snow layers with notable variations in density and hardness, causing stress accumulation in the snow layer at certain localities, increasing its instability. The temperature plays a decisive role in the formation of avalanches, as it can affect the snowpack stability in different ways, especially in the absence of snowfall, where the effect of the temperature on avalanches is particularly pronounced

and complex, e.g., temperature rise during or after a snowstorm can significantly impact the snowpack stability [5].

The snowy period in Aerxiangou starts in September and lasts until April, resulting in a snowy period of up to 8 months. The temperature is above 0 °C from September to October, so snow does not easily accumulate. After November, the temperature rapidly decreases and falls below 0 °C, the snow gradually accumulates under the effect of the temperature and heavy snowfall, and the snow thickness on slopes continuously increases. The precipitation amount during this period notably fluctuates, with a significant decline after November and reaching even as low as 0.6 mm in January, i.e., there is less snowfall in the region in January and significantly more precipitation afterward. The wind speed in the gully shows the same trend, which is significantly higher in March and April than in the other months of the snowy period. Figure 4 shows the month-by-month meteorological data for the past year (January 2022–April 2023) for Aerxiangou. According to the analysis of the meteorological data, the snow accumulation period can be divided into the prestorage and the late development stage, with January as the boundary. All factors except snow depth exhibit a downward trend at the prestorage stage, while all the meteorological factors exhibit an upward trend at the late development stage, greatly affecting avalanche triggering. Therefore, in this paper, we determined the average temperature (February to April), average snowfall (February to April), average snow depth (February to April), and average wind speed (February to April) as meteorological causative factors to analyze the effects of avalanche triggering.

2.5. Establishment of the Indicator System

Combined with environmental characteristics such as the topography, climate, and spatial distribution of avalanche hazards in Aerxiangou, eight disaster-causing factors, namely, the slope, elevation, surface cutting degree, surface roughness, average temperature, average snowfall, average snow depth, and average wind speed, were selected as index factors of the CF model. Referring to the literature, each factor was analyzed hierarchically. Graded analysis of the factors was conducted based on relevant studies [23,26–28]. Details of the grading process are provided in Table 2.

Through the DEM dataset, the 3D Analyst tool in ArcMap 10.8 software was used to extract the slope, average elevation, and standard deviation of the elevation in the study area, and the raster calculator was employed to statistically determine the surface cutting degree and surface roughness in the study area. The average wind speed, average snow depth, average snowfall, and average temperature from February to April were calculated from the meteorological monitoring data, and the spatial interpolation method was used to obtain meteorological remote sensing data for the study area. The above impact factors were processed under a uniform coordinate system and resampled into 15 m × 15 m analysis cells. A total of 31,077 rasters were used. The classification results for each contributing factor are shown in Figure 5.

2.6. Certainty Factor Model

The CF model is a probability function first proposed by Shorliffe and Buchanan [29], among others, and improved by Heckermann [30]. In this study, *CF* values were used to quantitatively determine the susceptibility zone of the hazard-causing factors and to analyze the likelihood of each type of avalanche-triggering factor. The *CF* value can be calculated as:

$$CF = \begin{cases} \frac{PP_a - PP_S}{PP_a(1-PP_s)}, \text{ if } \rightarrow PP_a \geq PP_s \\ \frac{PP_a - PP_s}{PP_s(1-PP_a)}, \text{ if } \rightarrow PP_a \leq PP_s \end{cases} \quad (1)$$

where PP_a is the conditional probability of an avalanche disaster event occurring in data class a, and PP_s is the a priori probability of an avalanche disaster event occurring within the entire study area A. Typically, PP_a can be expressed as the ratio of the number of avalanche disasters in the cell representing data class a to the area of the cell, while PP_s can be expressed as the ratio of the number of avalanche disasters to the study area as a whole.

The *CF* value range is $[-1, 1]$. A positive calculated result denotes an increase in the certainty of the event occurring, i.e., a high certainty of avalanche disaster occurrence, indicating that avalanche disasters are more likely to occur in this unit. Conversely, a negative calculated result denotes a reduction in the certainty of the event occurring, i.e., low certainty of avalanche disaster occurrence, indicating that this unit is not prone to avalanche disasters.

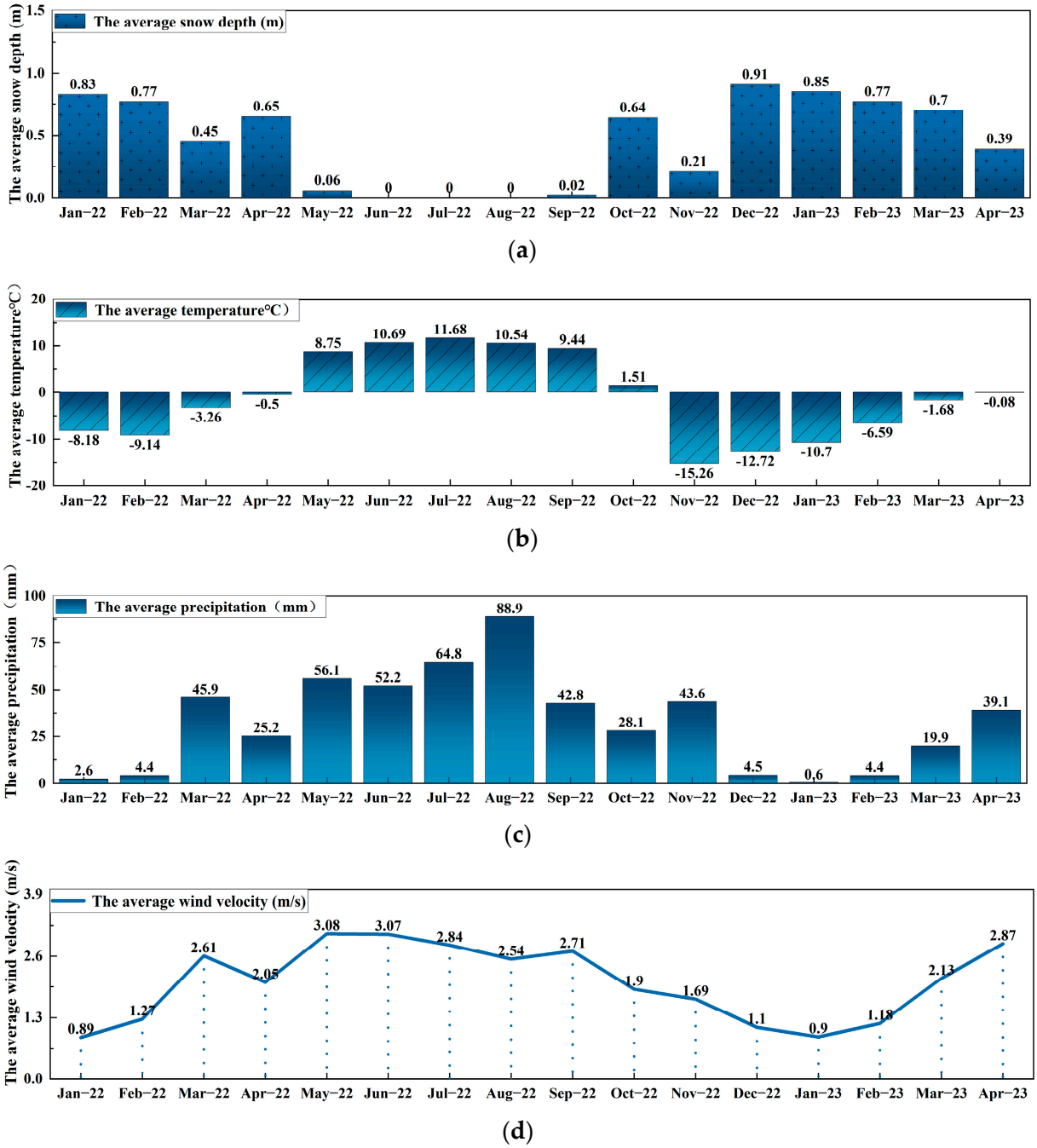

Figure 4. Monthly meteorological data for Aerxiangou for the last year (January 2022–April 2023) include (**a**) Average snow depth in Aerxiangou for the past year, month by month, (**b**) Average temperature in Aerxiangou for the last year, month by month, (**c**) Average precipitation in Aerxiangou for the last year, month by month, (**d**) Average wind speed in Aerxiangou for the last year, month by month.

Table 2. Classification (classification) of avalanche hazard causative factors.

Causal Factors	Grading
Slope/(°)	0~15, 15~30, 30~45, 45~60, >60
Elevation/m	<2400, 2400–2700, 2700–3000, 3000–3300, >3300
Surface cutting degree/m	0–30, 30–60, 60–90, 90–120, >120
Surface roughness	0–0.2, 0.2–0.4, 0.4–0.6, 0.6–0.8, >0.8
Average temperature/(°C)	<−14.2, −14.2~−12.3, −12.3~−10.4, −10.4~−8.5, >−8.5
Average snowfall/(cm)	<1, 1–8, 8–16, 16–24, >24
Average snow depth/(cm)	<3.5, 3.5~7.5, 7.5~11.5, 11.5~15.5, >15.5
Average wind speed/(m/s)	<1.2, 1.2–2.6, 2.6–4.1, 4.1–5.5, >5.5

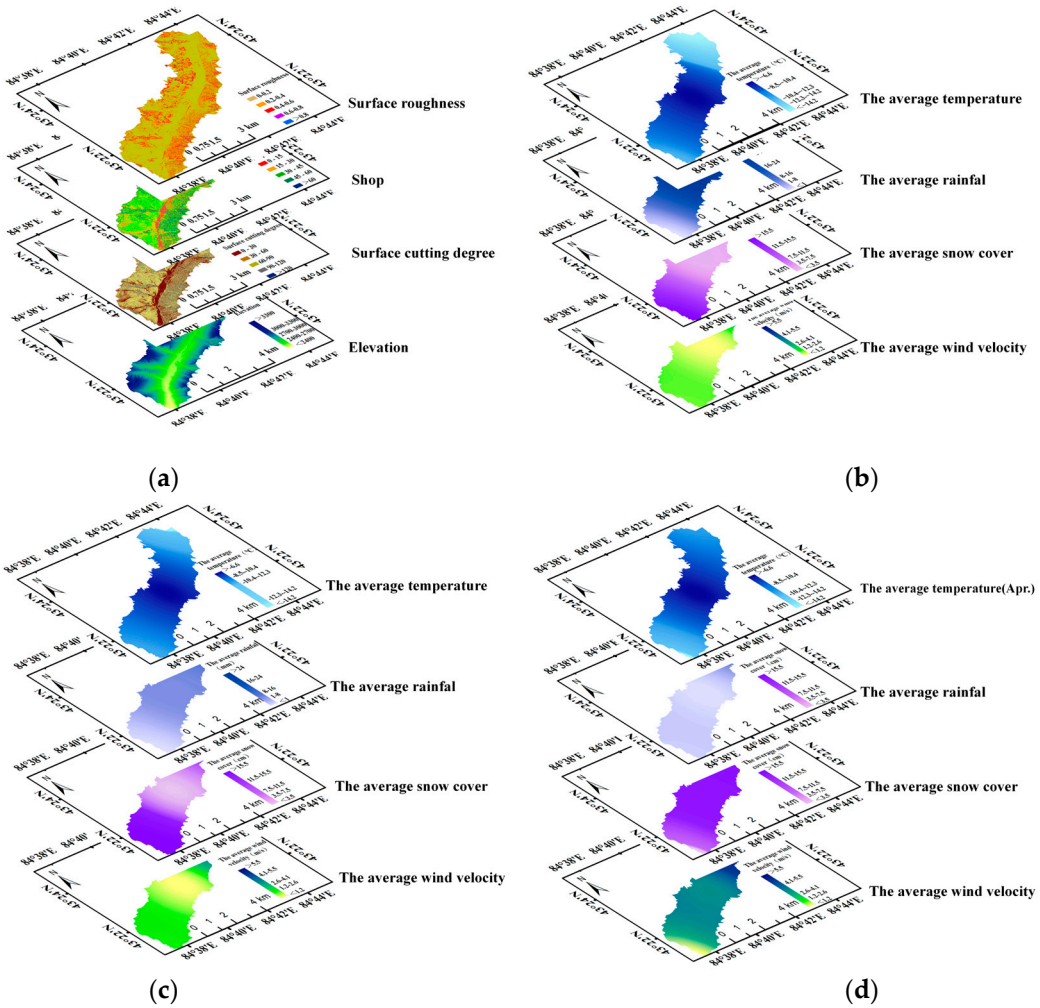

Figure 5. Hazard-causing factor classification map: (**a**) Topographic factor grading chart; (**b**) Meteorological factor classification chart (February); (**c**) Meteorological factor classification chart (March); (**d**) Meteorological factor classification chart (April).

2.7. Impact Index E

The degree of influence of a particular class of factors on avalanche triggered was captured overall using the influence index E, which can be expressed as:

$$E_i = CF_{(i,max)} - CF_{(i,min)} \quad (2)$$

where E_i is the influence index of a factor on avalanche triggering, $CF(i$ max) is the maximum value of the deterministic coefficient of avalanche (CF) for each category of the pregnant environment factor i, and CF (i min) is the minimum value of the deterministic

coefficient of the avalanche for each category of causative environmental factor *i*. Accordingly, we could analyze the influences of the various environmental factors on avalanche triggering as a whole, providing a quantitative basis for constructing a regional avalanche triggering analysis index system.

3. Analysis of the Aerxiangou Disaster Mechanism

3.1. CF Value Calculation and Analysis

3.1.1. Slope

The calculated CF values of the slope are provided in Table 3. A slope ranging from 15°~30° constrained the main disaster development area in February and March, and the CF values were 0.3984 and 0.1934, respectively. In comparison, the CF value in April within the 45°~60° interval was relatively high, close to 1, indicating the high frequency and certainty of disasters in April within this interval. The calculated CF values showed that avalanches tended to occur within the 15°~45° moderate slope range; namely, steeper slopes achieved a low snow accumulation capacity, while gentler slopes did not exhibit the necessary conditions to provide the driving force for downward sliding of the snow layer.

Table 3. Slope grading and CF value calculation results and analysis.

Classification /(°)	Quantity	PP_a	$PP_a(1-PP_s)$	$PP_s(1-PP_a)$	CF
	February/March/April				
0–15	0/0/0	0/0/0	—	1.5816/2.0787/0.2711	−1/−1/−1
15–30	6/8/0	1.327/1.7693/0	—	−0.639/−1.599/0.2711	0.3984/0.1934/−1
30–45	15/22/3	1.4041/2.0593/0.2808	—/—/0.2046	−0.639/−2.202/—	0.2778/0.0088/0.04729
45–60	13/13/3	3.8687/3.8686/0.8927	−2.25/−4.173/0.6507	—	0.0789/−0.4289/0.9553
>60	1/3/0	2.644/2.644/0	—/−4.3469/—	−2.6003/—/0.2711	−0.4085/0.13/−1

3.1.2. Elevation

The calculated CF values of the elevation are listed in Table 4. The occurrence of avalanche disasters in February was mainly concentrated between 2400 and 3300 m, in which the certainty of disaster occurrence from 2700~3000 m was lower, at −0.0198, close to 0. In March, avalanche disasters only yielded a positive CF value from 2400 to 2700 m, reaching only 0.1. Although the certainty of disaster occurrence in the region is increasing, the certainty is not high, resulting in a low occurrence frequency. In contrast, the elevation CF values of avalanche hazards in April were all negative, the certainty of avalanche occurrence was less correlated with elevation, and the certainty of occurrence was low.

Table 4. Elevation grading and CF value calculation results and analysis.

Classification /(m)	Quantity	PP_a	$PP_a(1-PP_s)$	$PP_s(1-PP_a)$	CF
	February/March/April				
<2400	0/0/0	0/0/0	—	2.76/3.63/4.72	−1/−1/−1
2400~2700	17/8/0	1.79/8.5634/0	—	−4.66/−2.74/0.2	0.2006/0.1/−0.1206
2700~3000	17/29/4	5.83/9.95/1.37	−1.548/−3.502/−1.67	—	−0.02/−0.018/−0.053
3000~3300	1/9//2	2.24/20.79/4.48	—/7015.228/−166.954	−5.9019/—/—	0.0087/−0.0233/−0.24
>3300	0/0/0	0/0/0	—	2.75/3.21/4.72	−1/−1/−1

3.1.3. Surface Cutting Degree

The surface cutting degree is closely related to avalanche occurrence, and the degree of mountain cutting directly affects the snow accumulation capacity of a given slope. The analysis of the calculated CF values in Table 5 revealed that the areas with a higher certainty of avalanche occurrence all occurred in intervals of a lower surface cutting degree. Avalanches in February were mainly concentrated within the 0~90 m interval of the surface cutting degree, with the highest CF value of 0.296 within the 60~90 m interval, and the

avalanche occurrence probability was the highest. The CF value in March reached 0.9264 within the 30–60 m interval, which is close to 1. Therefore, avalanches in March occurred more frequently in this interval. The CF values in April were positive only within the 0–30 m interval, reaching 0.281, with low certainty of hazard occurrence, indicating that the surface cutting degree was not the dominant control factor of hazard occurrence in April.

Table 5. Surface cutting degree grading and CF value calculation results and analysis.

Classification /m	Quantity	PP_a	$PP_a(1-PP_s)$	$PP_s(1-PP_a)$	CF
			February/March/April		
0~30	13/17/3	1.5498/2.026/0.3576	—/—/0.2553	−0.917/−2.25/—	0.12871/0.0734/0.281
30~60	14/12/3	1.2153/1.0416/0.2604	—/−1.2418/—	−12.39/—/0.2125	0.0365/0.9264/−0.121
60~90	8/13/0	8.4287/13.6965/0	−5.63/−17.4/—	—/—/0.285	0.296/−0.066/−1
90~120	0/4/0	0/31.64/0	—/37.72/—	1.67/—/0.285	−1/−0.78/−1
>120	0/0/0	0/0/0	—	1.67/2.19/0.285	−1/−1/−1

3.1.4. Surface Roughness

As the friction generated between snow particles and the lower bedding surface prevents the snow from sliding, only when the downward sliding force exceeds the resistance will the hillside snow body slide down to form a full avalanche. The ground surface roughness, therefore, directly influences the magnitude of the snow slide force. In February, as the snow amount on the slope accumulates but has not yet started to change qualitatively, the magnitude of the slope roughness is particularly important for triggering full avalanches. According to the calculated CF values in Table 6, the CF values in February were positive within the surface roughness interval from 0 to 0.6, in which the probability of avalanche occurrence is higher and full avalanches are highly likely to be triggered. The surface roughness was negative at all levels in March. As snow experiences metamorphosis at this time, the snow density increases, the cohesion and friction between snow particles increase, and the sliding force is reduced, so full-scale avalanches are less likely to occur under the influence of surface roughness. In April, the calculated CF values were positive only within the 0 to 0.2 surface roughness interval, reaching 0.7349, indicating a high frequency of avalanche hazards. At this time of year, as temperatures rise and the ground surface becomes increasingly exposed, a smooth surface emerges between the snow layer and lower bedding surface, reducing friction. When the lower bedding surface is smooth, the sliding force is higher than the resistance, facilitating the triggering of avalanches.

Table 6. Surface roughness grading and CF value calculation results and analysis.

Classification	Quantity	PP_a	$PP_a(1-PP_s)$	$PP_s(1-PP_a)$	CF
			February/March/April		
0~0.2	8/15/3	1.5571/2.92/0.5839	—/−3.15/0.4256	−0.8812/—/—	0.02782/−0.266/0.735
0.2~0.4	8/11/1	0.6105/0.8393/0.0763	—	−6.9854/−3.99/0.25	0.139/−0.217/−0.778
0.4~0.6	16/20/2	5.4165/6.77/0.677	−3.15/−7.3038/0.4934	—	0.502/−0.642/−0.823
0.6~0.8	3/0/0	3.7059/0/0	−2.1556/—/—	—/2.0787/0.2711	−0.9854/−1/−1
>0.8	0/0/0	0/0/0	—	1.5816/2.0787/0.2711	−1/−1/−1

3.1.5. Average Temperature

Temperature plays a decisive role in the formation of avalanches, especially in the absence of snowfall [5]. Warming enhances snow surface deformation down the slope, thus increasing the strain between the snowboard and the lower soft layer and the corresponding strain rate, yielding an unstable snow layer. According to the CF value calculation results provided in Table 7, avalanches were influenced by temperature changes in both February and March, leading to more avalanche disasters, with the calculated CF values reaching as high as 0.9845 within the −10.4 to −8.5 °C range in February and 0.9086 within the −14.2 to

12.3 °C range in March, indicating a higher certainty of avalanches and disasters. However, in April, a wide range of CF values between the zones, with the highest value reaching 0.9688 and the lowest reaching −1, indicate that the probability of avalanche occurrence in April is highly influenced by higher or lower temperatures.

Table 7. Average temperature grading and CF value calculation results and analysis.

Classification /(°C)	Quantity	PP_a	$PP_a(1-PP_s)$	$PP_s(1-PP_a)$	CF
	February/March/April				
<−14.2	7/4/3	2.7263/1.5578/0.9224	−1.5675/0.67336/0.2244	—	−0.7345/0.4134/0.9688
−14.2~−12.3	3/5/0	0.5674/0.9956/0	—/−1.0205/—	−2.7187/—/0.2104	−0.4234/0.9086/−0.2346
−12.3~−10.4	6/7/1	1.6305/1.902/0.2745	−0.9374/—/—	—/−1.8269/0.1958	−0.0592/0.0671/0.0233
−10.4~−8.5	5/14/1	1.315/3.682/0.26	—/−3.774/—	−0.993/—/0.1997	0.9845/−0.4391/−0.049
>−8.5	14/15/2	1.9577/2.0975/0.1438	—	−1.508/−2.222/0.231	−0.254/−0.0326/−0.555

3.1.6. Average Snowfall

Snowfall is the most important factor for forecasting large catastrophic fresh snow avalanches and an important indicator for classifying the risk of such avalanches [25]. The factors affecting fresh snow avalanches include the intensity and density of snowfall, as the rate of fresh snowfall settling affects the balance between the snow stress and the strength of the snow layer. Fresh snow avalanches are the most likely to occur in February. The slope occurs in a state of snow accumulation, and the accumulated snow is subject to increased stress down the slope due to snowfall settlement, leading to an increase in snow layer instability, which can trigger avalanches. According to the CF value calculation results in Table 8, the CF values in February showed an increasing trend, reaching 0.864 within the interval of >24 cm, with high certainty and frequency of avalanche occurrence. The CF values were positive within the snowfall interval below 16 cm in March and positive within the interval below 8 cm in April. Notably, the probability of avalanche occurrence was higher. During this period, due to snow accumulation on the slope after the snow period, the snow thickness reached a critical state, and a small amount of snowfall is sufficient to trigger destabilization of the shallow surface layer, leading to avalanche occurrence.

Table 8. Average snowfall grading and CF value calculation results and analysis.

Classification /(cm)	Quantity	PP_a	$PP_a(1-PP_s)$	$PP_s(1-PP_a)$	CF
	February/March/April				
<1	0/5/2	0/1.333/0.333	—/—/0.2433	1.6649/−0.676/—	−1/0.4586/0.2605
1~8	6/9/4	1.3435/2.9869/0.4045	—/−3.061/0.2953	0.57192/—/—	0.562/0.72/0.4557
8~16	12/20/0	1.1708/2.1547/0	—	−0.572/−0.66/0.699	0.864/0.0832/−1
16~−24	7/7/0	2.2097/2.6378/0	3.679/−3.06/—	0.993/—/0.6992	0.087/−0.79/−1
>24	12/4/0	4.687/0/0	−3.1167/—/—	1.508/−1.305/0.6992	−0.9696/−0.532/−1

3.1.7. Average Snow Depth

According to the calculated CF values provided in Table 9, as the slope area snow thickness involves a continuous accumulation process, February represents the early part of the snowpack period, the slope area snow thickness has not yet reached the critical state, and the average snow depth CF values at all levels are approximately 0, further indicating that this factor does notably control the occurrence of avalanche disasters in February. The CF values were more prominent in March and April than in February, peaking at 0.8436 within the 3.5~7.5 cm range in March and 0.5157 within the 7.5~11.5 cm range in April, with a stronger dominance and thus a higher probability of avalanche occurrence.

Table 9. Average snow depth grading and CF value calculation results and analysis.

Classification /(cm)	Quantity	PP_a	$PP_a(1-PP_s)$	$PP_s(1-PP_a)$	CF
	February/March/April				
3.5	0/17/1	0/2.36/0.2635	—/−2.418/—	1.5749/—/0.1988	−1/−0.1384/−0.0323
3.5~7.5	24/6/1	0.2711/1.378/0.3323	−0.9353/—/0.2426	−2.719/−0.766/—	−0.0555/0.8436/0.2567
7.5~11.5	3/10/4	0/1.787/0.433	—/—/0.3161	−0.9873/−1.594/—	0.1352/0.1493/0.5157
11.5~15.5	4/8/0	0.4737/3.654/0	−1.0894/−3.745/—	−0.993/—/0.27	−0.0476/−0.435/−1
>15.5	5/4/0	0.3113/0/0	—	−0.3863/2.0249/0.27	0.0853/−1/−1

3.1.8. Average Wind Speed

The wind is second only to fresh snowfall as a meteorological factor influencing avalanches. Wind-blown snow settles at a high rate, and wind speed variation causes high variation in the density and hardness of the snow layer formed by wind-blown snow and induces local stress accumulation in the snow layer, thus increasing the snow layer instability. According to the CF value calculation results provided in Table 10, the positive CF values of the wind speed from February to April did not vary much, and only in April did the CF value between 2.6 and 4.1 m/s exceed 0.5, reaching 0.6175. This finding indicates that wind speed is not a major control factor of avalanche triggering and that other factors should be jointly considered. For example, when snow falls, even at low wind speeds, wind-blown snow still exhibits a high starting force, carrying more snow particles for redistribution, thus causing localized settling of the snowboard and snow layer destabilization, promoting avalanche triggering.

Table 10. Average wind speed grading and CF value calculation results and analysis.

Classification /(m/s)	Quantity	PP_a	$PP_a(1-PP_s)$	$PP_s(1-PP_a)$	CF
	February/March/April				
<1.2	0/0/1	0/0/0.2453	—	2.025/−1.1296/0.237	−1/−1/−0.1213
1.2~2.6	23/7/4	1.4304/0.4621/0.3494	—/−1.0205/0.255	1.0893/—/—	0.1757/0.3103/0.3113
2.6~4.1	3/9/1	1.6995/3.1861/0.4916	—/—/0.3588	−4.4268/—	−0.1274/−0.192/0.6175
4.1~5.5	1/14/0	0.5358/4.271/0	—/−4.377/—	−1.1016/—/0.2699	0.1311/0.1854/−1
>5.5	8/15/0	3.1852/0/0	−1.8313/—/—	—/2.0249/0.2699	−0.8792/−0.8536/−1

3.2. Analysis of the Degree of Influence of the Hazard-Causing Factors

The analysis in the previous section clearly indicates that the different categories of the same hazard-causing factors show different certainties for triggering avalanche hazards. The range of the deterministic coefficient values for avalanches according to the different categories, i.e., the avalanche influence index E, provides an overall approximation of the degree of influence of a given factor on avalanche triggering, as indicated in Table 11.

The curve based on the type of avalanche hazard-causing factor and the degree of influence on the avalanche influence index E is shown in Figure 6, which reveals that factors such as the slope, elevation, and average air temperature control the spatial distribution of avalanches in the study area. In February, the E values of the mean snowfall and mean average temperature were significantly higher than those of the other causal factors, at 1.8336 and 1.719, respectively, with a clear dominance and high degree of influence. At this time, the mountain slope is in the accumulation of snow thickness process. The average snowfall and average temperature are meteorological factors providing sufficient material conditions for the occurrence of avalanches—snow particles, in collaboration with other factors, induced mainly small and medium-sized avalanches.

Table 11. Degree of influence of the avalanche hazard-causing factors.

Serial Number	Causal Factors	Degree of Influence €	Max.	Min.
			February/March/April	
1	Slope	1.3984/1.1934/1.9553	0.3984/0.1934/0.9553	−1/−1/−1
2	Elevation	1.2006/1.1/0.9462	0.2006/0.1/−0.0538	−1/−1/−1
3	Surface cutting degree	1.296/1.9264/1.281	0.296/0.9264/0.281	−1/−1/−1
4	Surface roughness	1.502/0.734/1.7349	0.502/−0.266/0.7349	−1/−1/−1
5	Average temperature	1.719/1.9086/0.4015	0.9845/0.9086/0.1669	−0.7345/−1/−0.2346
6	Average snowfall	1.8336/1.2486/1.4557	0.864/0.4586/0.4557	−0.9696/−0.79/0.4557
7	Average snow depth	1.1352/1.8436/1.5157	0.1352/0.8436/0.5157	−1/−1/−1
8	Average wind speed	1.0549/1.1639/1.6175	0.1757/0.3103/0.6175	−0.8792/−0.8536/−1

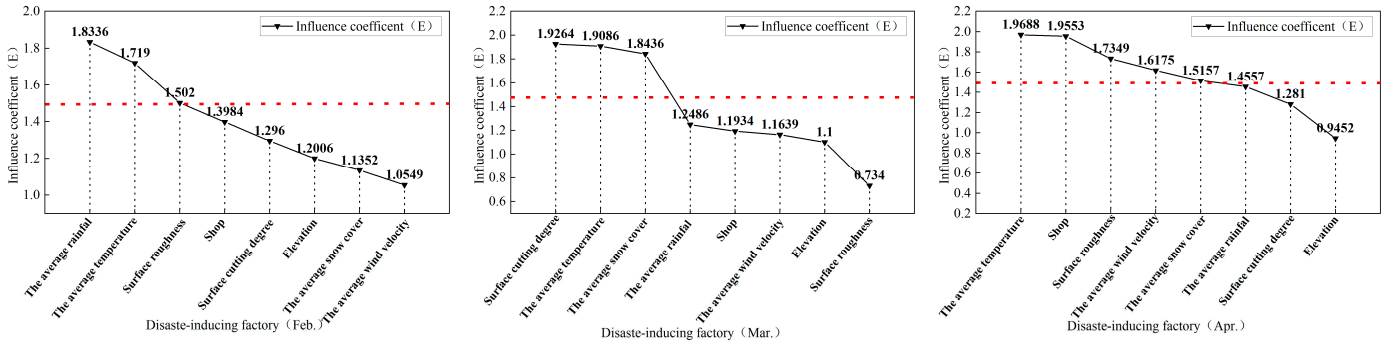

Figure 6. Degree of influence of the hazard-causing factors on avalanche.

The main control factors of avalanche hazards in March were the surface cutting degree, average temperature, and average snow depth, with index values above 1.8, while the least influential factor was surface roughness, with an index value of 0.734. The reason is that during this period, the snow thickness on the slope approaches critical value, but the deep snow and subsurface have reached a relatively stable state. Therefore, avalanches induced by topographic and meteorological factors are mostly surface avalanches.

In April, there were four hazard-causing factors with E values above 1.5, namely, the average temperature, slope, surface roughness, and average wind speed, indicating a high degree of influence. The hazard-causing factors with index values below 1 were the surface cutting degree and elevation. The main reason for this is that during this period, the temperature rises or falls significantly, and the magnitude of the change not only directly affects the nature and distribution of snow particles but also changes the friction between the lower bedding surface and the contact surface of the snow layer. The external force of wind speed stresses the snow layer, causing some local accumulation and then triggering the avalanche, and, most dangerously, impacts a wide range of wet snow avalanches.

4. Characteristics of Avalanche Activity in Aerxiangou

4.1. Basic Characteristics

Aerxiangou avalanche disasters are mainly concentrated on the northern and southern sides of the valley. The southern side of the avalanche point is far from the Y029 country road, and there are tall trees, reducing the impact. The northern side of the folded mountain block is the primary disaster-prone environment. It is located close to the Y029 country road, and disasters frequently occur that can cause road and other major infrastructure losses. As indicated in Table 12 (statistical results of avalanche hazard characteristic values), in the winter and spring of 2023, avalanche hazards frequently occurred in the Aerxiangou section due to different hazard-causing factors, with avalanche flows flowing across the road and accumulating on a large scale, creating multihazard sites. The specific locations are shown in Figure 7.

Table 12. Statistical results of avalanche disaster characteristic values.

No.	Type	Month	Size of the Stockpile Area (m^2)	Critical Thickness of Snow on Slopes (cm)	Slope (°)	Surface Morphology (Roughness)	Vegetation Type
1#	Slope type	February	6 m × 1.2 m × 1.2 m	0.34	30°~40°	Fine snow particles	Rocky slopes
2#	Slope type	March	14 m × 3 m × 1.7 m	0.53	50°	Fine snow particles	Short meadow
3#	Gully slope type	March	150 m × 8 m × 1.7 m	0.79	26°~35°	Fine snow particles	Rocky slopes
4#	Groove type	April	12 m × 3 m × 1.8 m	0.79	26°~35°	Loose snow clumps	Short meadow
5#	Groove type	February	3 m × 1.5 m × 1.5 m	0.59	40°~55°	Fine snow particles	Rocky slopes

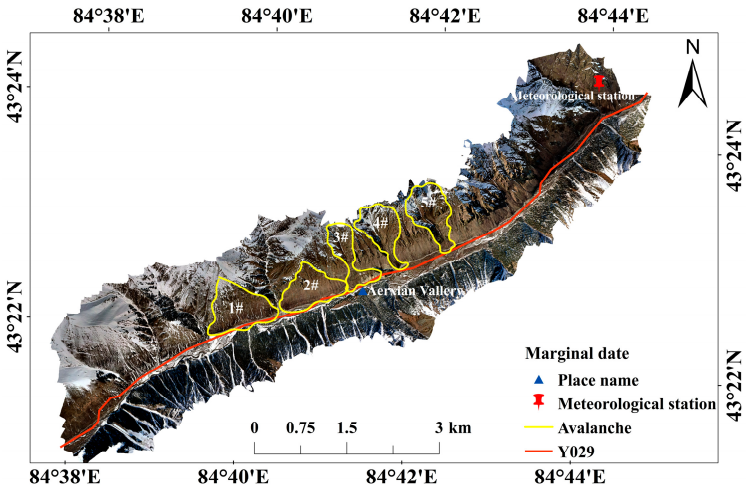

Figure 7. Map of multiple avalanche points.

4.2. Analysis of the Avalanche Motion Process

It was found that avalanche area 4# is a typical multi-avalanche hazard area. Between February and April, under the prominent effect of the different disaster-causing factors, full-layer fresh snow avalanches, surface snow avalanches, and full-layer wet snow avalanches were triggered. The actual situation at the site is shown in Figure 8. Since the snow layer at this point is consistent with the slope inclination, the occurrence nature of surface and full-layer avalanches is the same. At the same points on the surface of the snow layer under the action of the same stress, the compressive and tensile stresses are not parallel to the slope when the shear stress increases from the snow layer surface to the ground surface. The ground supports the snow body under the superposition of compressive and shear stresses. Under these two types of stresses, the snow body undergoes continuous shear deformation, which occurs parallel to the creep surface. When the snowfall level in February is high, the self-weight of the upper snowpack increases and gradually moves downward, and the stress needed to trigger a full-layer avalanche first reaches the limit value at point A. If a rupture occurs, the back snow layer imposes tensile stress down along the slope, and due to the change in the stress of the stabilized slope, the load near the rupture surface increases, and the range expands, while a full-layer fresh snow avalanche is formed. The stress diagram is shown in Figure 9a. Based on the measured density in onsite exploratory pits, the snow on the slope in March comprised dense fine and medium snow in the upper part and coarse snow and deep frost in the lower part in the continuous accumulation process. The snow layer properties are summarized in Table 13 and Figure 8d. Whereas coarse snow and deep frost are easily compressed downward by forces perpendicular to the slope when the snow on the surface is subjected to temperature gradient-induced variation, the surface snow becomes stronger than the lower snow, the load increases, the snow layer sinks, the surface layer fractures, and a surface snow avalanche is formed. The stress diagram is shown in Figure 9b. Temperature also plays a role in new snowfall. Notably, when the temperature is close to or slightly above 0 °C in April, the water content in snow increases, the intensity significantly declines, meltwater penetrates the ground, and the snow layer

near the ground becomes wet and forms a sliding surface, which in turn triggers a full wet snow avalanche. The stress diagram is shown in Figure 9a.

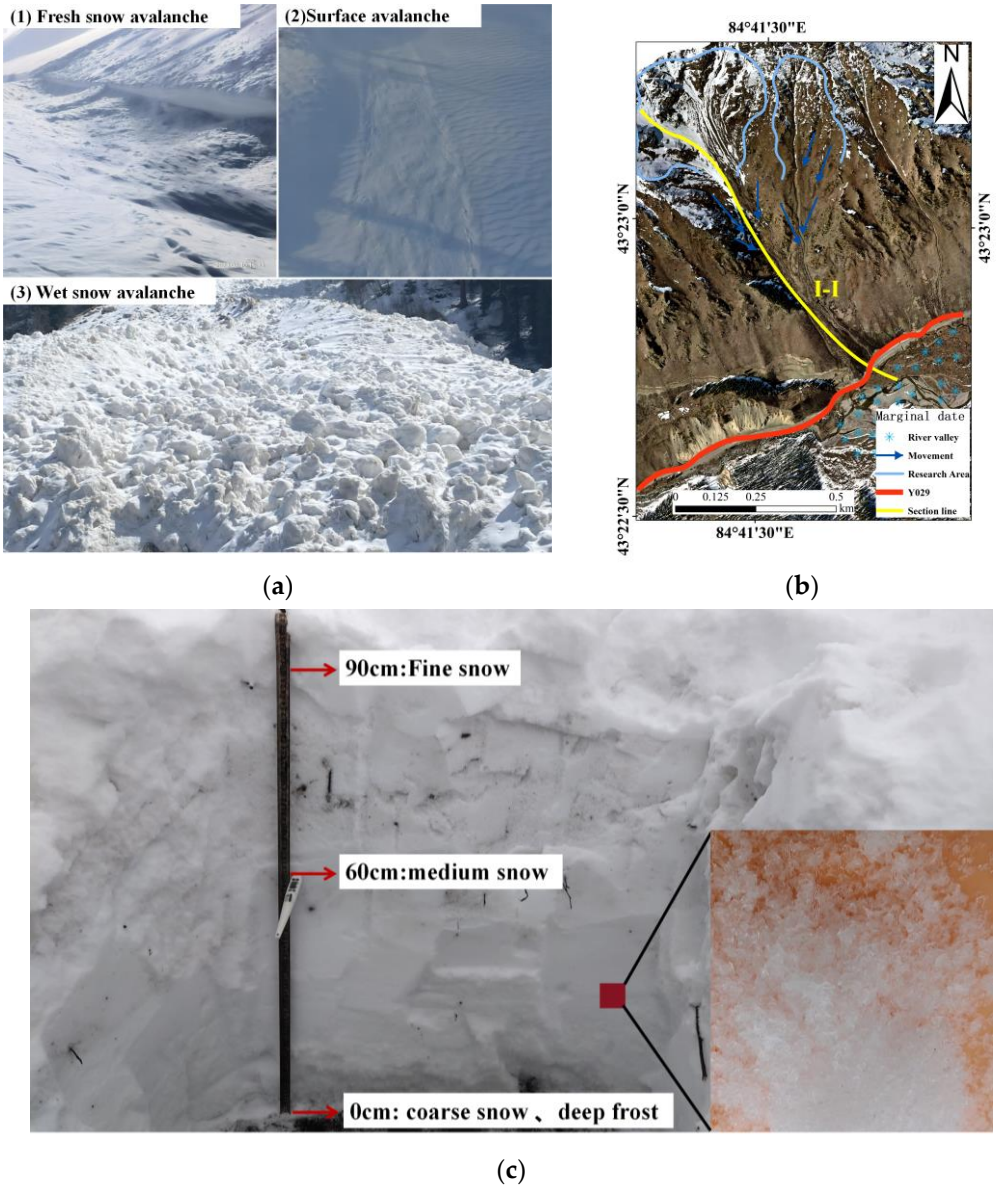

Figure 8. Avalanche disaster site 4#:(**a**) Disaster situation at the site; (**b**) Study area; (**c**) Cross-sectional view of the exploratory pit.

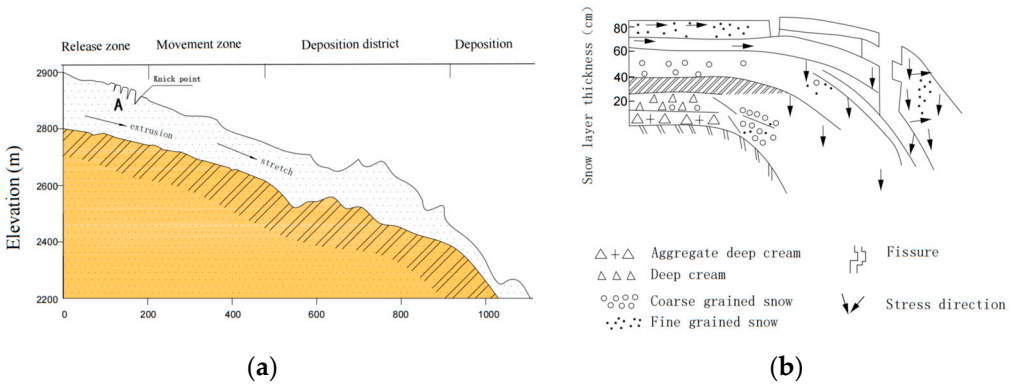

Figure 9. Illustration of the snow stress: (**a**) Full-layer avalanche; (**b**) Surface avalanche.

Table 13. Snow layer characteristics.

Snow Layer Thickness/(cm)	Snow layer Temperature/(°C)	Snow Layer Density/(g-cm^{-3})	Characteristics
100–90	−4	119	Fine snow
90–70	−5.6	283	Medium snow
70–65	−5.2	337	Medium snow
65–50	−3.5	352	Coarse snow, deep frost
50–45	−1.4	402	Coarse snow, deep frost
43–30	−0.8	417	Coarse snow, deep frost
<30	0.2	452	Coarse snow, deep frost

4.3. Analysis of the Simulation Results

To further identify the activity characteristics at multiple avalanche hazard sites, the RAMMS-avalanche model was used to control parameters such as the release depth and snow density to distinguish three avalanche material characteristics, and at the same time, considering that the secondary avalanche paths within the same area are affected by the deposition of previous avalanche flows, the simulations were driven by snow deposition in the DEM to ensure closer simulation results to the actual conditions.

The main cause of avalanche triggering due to fresh snow totality is the decomposition of the gravitational forces applied to the slope into stresses parallel to the slope and positive pressures perpendicular to the slope due to the continuous accumulation of snow on the slope. The lower snow layer, under gravity's action, tends to slide down the slope when a certain point of snow layer stress reaches the limit value, causing a rupture at the rear of the snow layer extrusion. At the same time, the layer's tensile stress along the downslope, which stabilizes the slope surface stress, changes. The rupture surface of the load near the surface becomes larger, along with the scope of the expansion, resulting in a decline in the snow layer greater than its resistance to avalanche triggering. This results in a critical thickness h_k of snow on the slope area of the hillside, as shown in Equation (3). When the slope area snow thickness reaches the critical thickness value, the sliding force and resistance of the snow layer are in equilibrium. At this time, if the increase of the snow thickness or uneven distribution of the snow layer stress will lead to the settlement of the snow layer, causing the slide collapse. Therefore, the critical thickness h_k is invoked in this study to determine the depth of full-layer fracture of fresh snow avalanches.

$$h_K = \frac{c}{\tau(\sin\alpha - \cos\alpha \times \mathrm{tg}\phi)} \tag{3}$$

h_k is the thickness of the snowpack on the hillside; C is the cohesion between the snow and the slope surface; ϕ is the angle of internal friction between the snow and the ground (°); τ is the density of the snowpack (g·cm^{-3}); and α is the gradient of the hillside (°).

Since the values in Equation (3) (cohesion, angle of internal friction, snow density, slope) are all related to snowpack and slope characteristics. Combining the actual situation of the site in the study area with the results of the analysis of the physical and mechanical strength of different types of snow derived from the study of the physical properties of seasonal snow in the Tien Shan mountainous region by Hu Ruji [31–33] and others, the value of the numerical values in Equation (3) is determined; in which the slope gradient of the mountain slopes is analyzed according to the terrain. The specific physical properties are taken as shown in Table 14.

Table 14. Physical properties of snow cover.

Snow Type	Cohesion/(g·cm^{-2})	Internal Friction Coefficient	Densities/(g·cm^{-3})	Breaking Strength/(g·cm^{-2})
Fresh snow	5	0.22	0.15 (measured value)	2.8

Depth of rupture value for fresh snow surface and full wet snow avalanches are based on field measurements. Specific simulation parameters such as snow density and friction coefficient were matched based on measured avalanche values in the study area and combined with the recommended values of model parameters to apply to the study area. The specific simulation parameters are listed in Table 15.

Table 15. Numerical simulation parameters (according to Qiu Jiaqi [34], Schaerer [10], and Buser et al. [32]).

Time	Snow Type	Type	Measured Density/(g·cm^{-3})	Depth of Rupture/(m)	Friction Coefficient	
February	Fresh snow	Full-layer avalanche	150	0.79 (threshold value)	Return period: 10 years	μ: 0.34 ξ: 1250
March	Fresh snow	Surface avalanche	215	0.16 (measured snow thickness increment)		
April	Frozen medium-grained snow	Full-layer wet avalanches	435	0.3 (measured average snow thickness)		

According to the simulation results of the characteristic values for each motion process at avalanche point 4# under different periods, as shown in Figure 10, the February avalanche motion at avalanche point 4# exhibited a short start-up time and a high sliding speed. The flow velocity was higher than the simulation results of the March and April avalanche movements as a whole, and the movement process lasted 13.6 s, with the maximum flow velocity reaching 21.9 m/s. Accumulation was mainly concentrated in the bottom of the gully valley and the river valley area, and the impact range was roughly the same as the actual range, with the maximum accumulation thickness in the river valley area reaching 9.17 m. The maximum pressure was observed in the left movement area at approximately 72 kPa. The simulation process of avalanche movement in March and April was greatly affected by the topographic relief due to the consideration of deposition and superimposed deposition in the DEM. Compared to the results of the three eigenvalue simulation campaigns, the changes in the area of the influence of avalanche flow were mainly concentrated in the release and flow zones. The gullies in the depositional area are well-developed, narrow, and deep, and there are no other gullies, so there is no significant change in the influence range of the depositional area. In contrast, the value of the change in the kinematic eigenvalue is larger. According to the I-I motion eigenvalue change curve graph of the lower profile under different periods, as shown in Figure 11, the peak of the accumulation height in March and April emerged earlier in the deposition process under the influence of sedimentation. Still, the overall flow height was smaller than in February due to the smaller release amount. The maximum flow height was approximately 8 m in March and April, and it occurred in the low-accumulation area of the slope. The pressure magnitude is largely due to density change, which affects the change in the snow mass. Therefore, the pressure eigenvalue graph showed that the impact force is significantly higher in April than in March and February, and the maximum value can exceed 60 kPa.

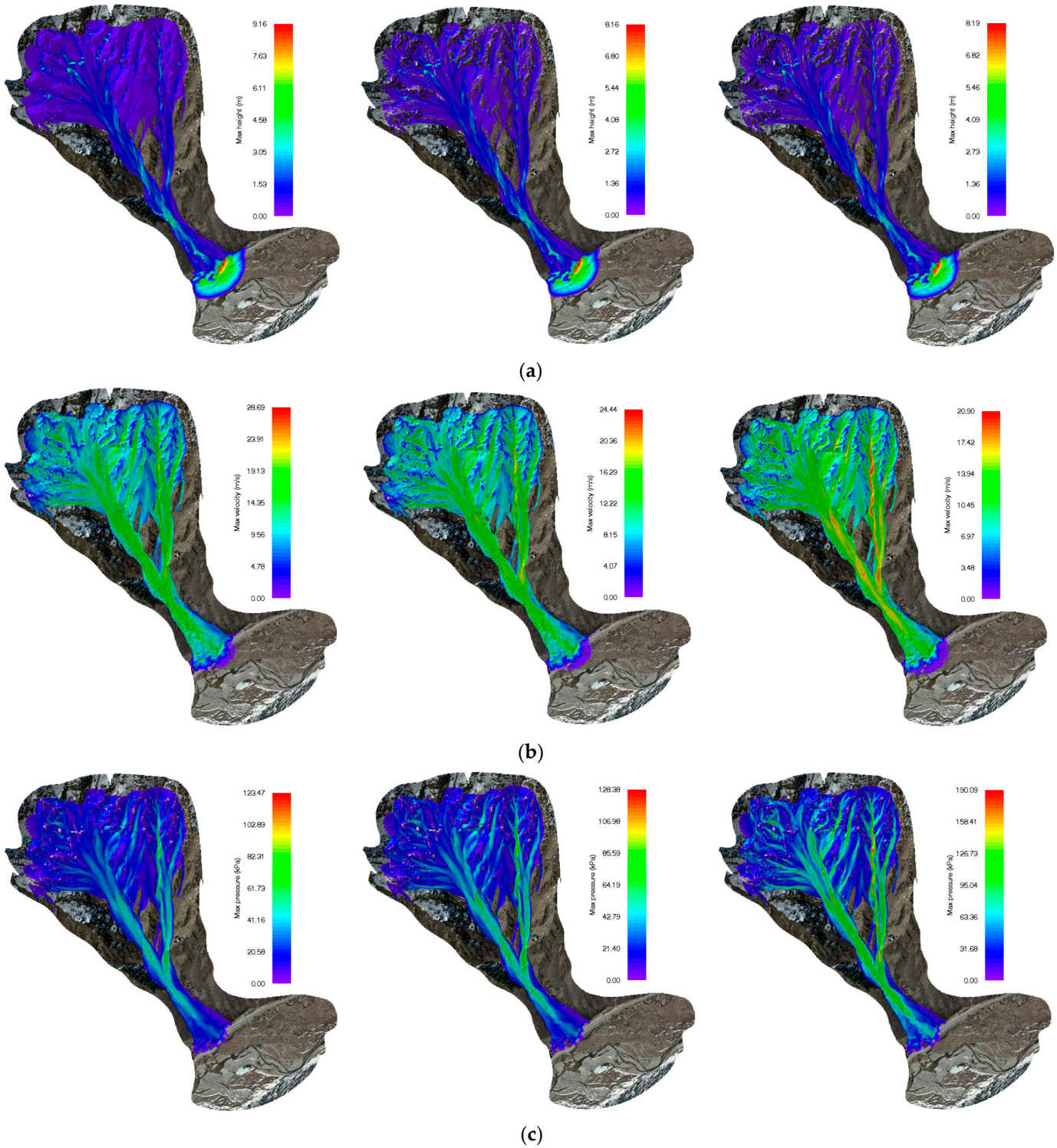

Figure 10. Characteristic values of the movement process at avalanche point 4# under the different periods: (**a**) Maximum height; (**b**) Maximum velocity; (**c**) Maximum pressure.

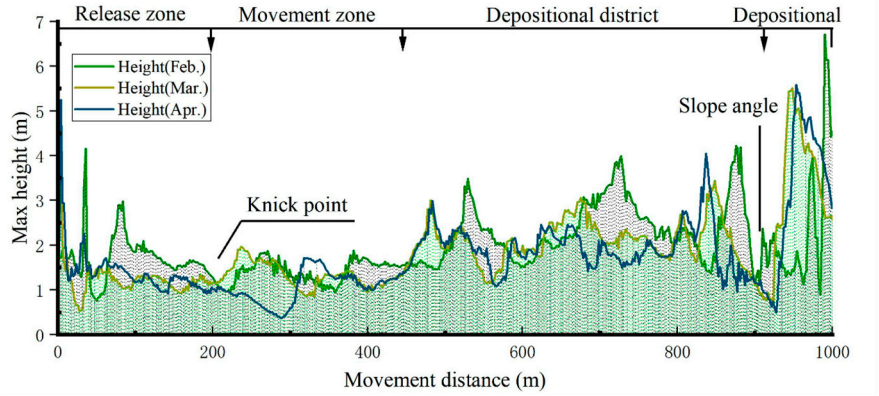

(**a**)

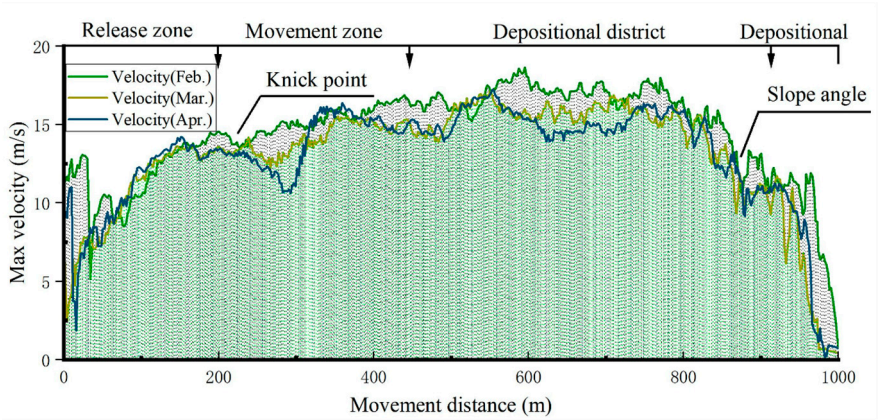

(**b**)

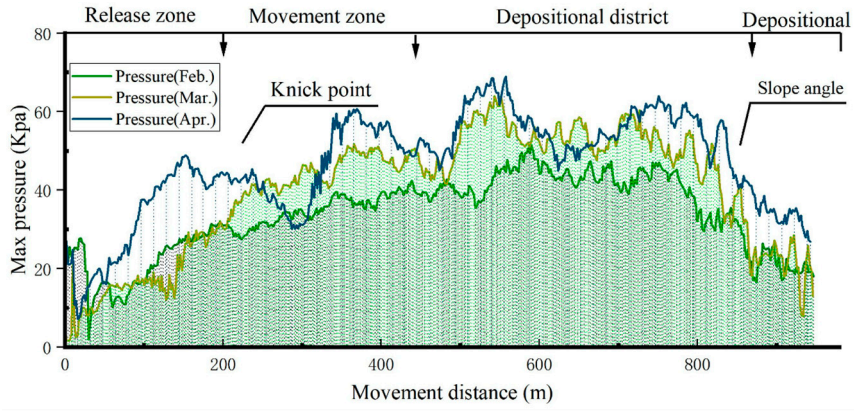

(**c**)

Figure 11. Variation curves of the profile I–I motion eigenvalues under the different periods: (**a**) Flow height variation curve of profile I–I under the different periods; (**b**) Flow velocity curve of profile I-I flow under the different periods; (**c**) Pressure the curve of profile I–I under the different periods.

5. Discussion

In the study of the mechanism of avalanche disasters, the physical and mechanical nature and trends of the dynamic change process from the steady state to unstable sliding are analyzed under the joint action of the inherent geological conditions of the mountain area and meteorological and human-induced factors, which provides a theoretical basis for avalanche prediction and early warning and effective prevention [26,35]. At present, many scholars have examined various avalanche-causing mechanisms, such as the analysis of avalanche formation conditions and influencing factors [28,36,37], analysis of snow layer forces [38], analysis of snow mechanical properties and spatial and temporal variation

patterns [27,39,40], and analysis of the impact of skiing on the snow layer stability [10,41]. Avalanche hazards are most likely to occur in parts of mountain slopes with favorable snowfall conditions and slopes ranging from 35° to 45°, and these parts of mountain slopes are key potential hazard sites. After clarifying the main types of disaster occurrence, activity characteristics, and movement characteristic values, targeted development of measures for early identification and prediction of disaster hazards could further improve the efficiency of disaster prevention and mitigation efforts and reduce the direct losses caused by avalanche disasters. In this paper, we analyzed avalanche-triggering factors in the small-scale area of Aerxiangou, aiming to reveal the disaster-causing mechanisms and activity characteristics at multiple avalanche hazard sites in the study area and to provide a reliable scientific basis for avalanche disaster prevention and control.

Based on several field surveys aimed at exploring the distribution and scale of avalanches, the correlation between eight hazard-causing factors and the number of avalanches was studied using the CF model, the influence index (E) of each hazard-causing factor was derived using CF values, and the main control factors of avalanche triggering under different periods were proposed. Notably, different categories of avalanches could be induced under the influence of the main control factors under different periods, which is consistent with the findings of Wenlinke et al. [5] Multiple factors control avalanche triggering, and different categories of avalanches can be formed for different reasons. Since disaster triggering results from multiple factors, there are complex interrelationships among the considered factors. Zhou Jin et al. [42] used the geographic detection method to reveal that the results of a two-by-two interaction analysis of causative factors could be enhanced, with a significantly higher impact degree and a higher probability of disaster occurrence under the interaction of factors. Bruce Jamieson et al. [43] suggested that there exists a stronger correlation between the temperature and snow thickness than with other factors and that the snow thickness is the main factor controlling the occurrence of slab avalanches. In this paper, only eight influential factors with a notable impact on avalanche triggering were independently analyzed to achieve factor elucidation. The secondary role of factors and the interaction among factors should be studied further.

To identify the activity characteristics at multiple avalanche hazard sites, theory and simulation experiments were combined to determine the formation process of avalanches of various categories under the influence of the main controlling factors. The RAMMS-avalanche simulation experiment revealed that, based on considering depositional effects on secondary avalanche paths, the influence range of the avalanche flow deposition area changes slightly. In contrast, the avalanche path greatly changes in the movement area, and the different categories of avalanches exhibit high variability in their kinematic eigenvalues. Overall, wet snow avalanches are more hazardous and generate higher pressure. Fresh snow avalanches exhibit shorter start-up times and higher sliding speeds, while the difference in the avalanche sliding surface (the whole and surface layers) mainly manifests in the difference in the flow height. The movement paths derived from the simulation results conform to the actual situation of avalanche activity. Therefore, the RAMMS-avalanche model is a very effective tool for simulating avalanche movement and has promising application prospects. However, when this model is used in the design of disaster prevention and mitigation engineering, the destructive force of the turbulent flow structure formed by the high-speed movement of snow particles should not be ignored. On this basis, disaster prevention and mitigation work should be further studied to determine a certain proportion of the impact range buffer zone, and the characteristic value of protection engineering design work should be prioritized over simulated design values.

Recently, regarding avalanche hazards, researchers have focused on prevention and mitigation efforts at sites where hazards have already occurred, ignoring the issue of potential avalanche sites. As a result of global climate change, extreme weather events are occurring frequently, especially extreme snowfall, wind-blown snow, and a sudden rise in spring temperatures, resulting in avalanches frequently occurring in areas not traditionally prone to avalanches in recent years. Mechanisms such as disaster risk identification and

early warning have not been adapted to the new requirements of the new situation, which could cause incalculable losses to the safety of people's property and infrastructure construction. Therefore, by emphasizing risk identification and assessment management of avalanche hazards at highways, scenic spots, and important infrastructure areas, we could effectively avoid disasters and provide a scientific basis for infrastructure construction and planning in disaster areas.

6. Conclusions

Based on remote sensing interpretation and field investigation, in this paper, we established a spatial distribution map of avalanche hazards in Aerxiangou, applied the CF model to analyze various hazard-causing factors in the avalanche-prone environment in the study area, quantified the degree of influence of the different disaster hazard-causing factors on avalanche triggering, derived the main control conditions for avalanche occurrence under different periods and examined the activity characteristics at multiple avalanche sites. The study conclusions are as follows:

(1) From the perspective of the degree of influence, in February, the E values of the average snowfall and average temperature were significantly higher than those of the other hazard-causing factors, reaching 1.8336 and 1.719, respectively, indicating that these two factors were the main control factors of the occurrence of avalanche disasters in February. The main control factors of avalanche disasters in March were the surface cutting degree, average temperature, and average snow depth, all with index values higher than 1.8. In April, the number of hazard-causing factors with an E-value higher than 1.5 reached four, including the average temperature, slope, surface roughness, and average wind speed, and their control was obvious;

(2) Aerxiangou triggers full-layer fresh snow avalanches, surface snow avalanches, and full-layer wet snow avalanches due to the dominant role played by different causative factors. In February, under the accumulative effect of heavy snowfall, the snowpack is fractured, thus destabilizing slopes and generating full-layer fresh snow avalanches. The snow on the slopes in March formed a body of snow that was dense on top and loose on the bottom as it continued to accumulate. When the surface snow is subjected to temperature gradient-induced metamorphism, the strength becomes higher than that of the lower snow, the load increases, the snow layer sinks, and the surface layer ruptures to form a surface avalanche. The temperature in April is close to or slightly higher than 0 °C, the water content in snow rapidly increases, meltwater infiltrates into the ground, the snow layer near the ground becomes saturated, and the formation of a sliding surface triggers a full-layer wet snow avalanche;

(3) The simulation experiments using the RAMMS-avalanche model revealed that, based on the consideration of depositional effects on the secondary avalanche paths, there occurred slight variation in the extent of influence within the avalanche flow accumulation zone and high variation along avalanche paths within the kinematic zone. There was high variability in the kinematic eigenvalues of the different avalanche types. Overall, wet snow avalanches are more hazardous and produce higher impact forces, fresh snow avalanches exhibit shorter start-up times and higher sliding speeds, and the difference in the avalanche sliding surface (whole and surface layers) is mainly manifested as a flow height value difference. Moreover, the movement paths derived from the simulation results conform to the actual situation of avalanche activity.

Author Contributions: Conceptualization, J.L., T.Z., B.W. and C.H.; methodology, J.L., T.Z. and Z.Y.; software, S.Y. and T.Z; validation, T.Z., S.Y. and X.S.; formal analysis, T.Z. and S.Y.; investigation, J.L.; T.Z., C.H., B.W., Z.Y., X.S. and S.Y.; resources, J.L. and C.H.; data curation, T.Z., Z.Y. and C.H. writing—original draft preparation, J.L. and T.Z; writing—review and editing, J.L. and T.Z.; visualization, Z.Y.; supervision, C.H.; project administration, Z.Y. and B.W.; funding acquisition, J.L. and C.H. All authors have read and agreed to the published version of the manuscript.

Funding: This research was funded by the key Science and Technology projects in the transportation industry, grant number 2022-ZD6-090; the Xinjiang Transportation Science and Technology Project, grant number 2022-ZD-006; the Xinjiang Jiaotou Group's 2021 annual "unveiling of the list of commanders" science and technology project, grant number ZKXFWCG2022060004; and the Xinjiang Transportation Design Institute Science and Technology R&D Project, grant number KY2022021501.

Conflicts of Interest: The authors declare no conflict of interest.

References

1. Bründl, M.; Etter, H.J.; Steiniger, M.; Klingler, C.; Rhyner, J.; Ammann, W.J. IFKIS—A basis for managing avalanche risk in settlements and on roads in Switzerland. *Nat. Hazards Earth Syst. Sci.* **2004**, *4*, 257–262. [CrossRef]
2. McClung, M.D. Characteristics of terrain, snow supply, and forest cover for avalanche initiation caused by logging. *Ann. Glaciol.* **2001**, *32*, 223–229. [CrossRef]
3. Ebert, P.A.; Morreau, M. Safety in numbers: How social choice theory can inform avalanche risk management. *J. Adventure Educ. Outdoor Learn.* **2023**, *23*, 340–356. [CrossRef]
4. Qin, Q.; Li, X.; Hao, J.; Zhang, B.; Li, Q.; Gong, Z. Avalanche hazard zoning and spatial and temporal dynamics in the Tianshan Mountains, China. *J. Nat. Hazards* **2023**, *32*, 117–124.
5. Wen, L.; Xiang, L.; Cai, Y.; Su, F.; Yan, Z. Research on the formation mechanism of avalanches. *Mt. Res.* **2016**, *34*, 1–11.
6. Wang, Y. Dry-snow avalanches in China. *J. Glaciol. Geocryol.* **1986**, *8*, 381–387.
7. Qiu, J.; Deng, Y. Avalanches in the Bogda Peak area of Tianshan Mountain. *J. Glaciol. Geocryol.* **1983**, *5*, 227–234, 255–256.
8. Wang, S.; Ren, J. A review of the progress of avalanche hazard research. *Prog. Geogr.* **2012**, *31*, 1529–1536.
9. Hao, J.; Li, L. Research progress and the prospect of snow avalanche disaster prevention and control. *J. Glaciol. Geocryol.* **2022**, *44*, 762–770.
10. Schweizer, J.; Jamieson, B. Snow cover properties for skier triggering of avalanches. *Cold Reg. Sci. Technol.* **2001**, *33*, 207–221. [CrossRef]
11. Maggioni, D.; Gruber, U. The influence of topographic parameters on avalanche release dimension and frequency. *Cold Reg. Sci. Technol.* **2003**, *37*, 407–419. [CrossRef]
12. Hao, J.; Mind'Je, R.; Liu, Y.; Huang, F.; Zhou, H.; Li, L. Characteristics and hazards of different snow avalanche types in a continental snow climate region in the Central Tianshan Mountains. *J. Arid. Land* **2021**, *13*, 317–331. [CrossRef]
13. McClung, D.M.; Schweizer, J. Skier triggering, snow temperatures, and the stability index for dry-slab avalanche initiation. *J. Glaciol.* **2017**, *45*, 190–200. [CrossRef]
14. Ancey, C. *Snow Avalanches*; Springer: Berlin/Heidelberg, Germany, 2001.
15. Gratton, D.B.E. Meteorological triggering scenarios of tree-ring-based snow avalanche occurrence on scree slopes in a maritime climate, Eastern Canada. *Phys. Geogr.* **2020**, *41*, 3–20. [CrossRef]
16. Wang, Z.H.; Hu, Z.W.; Zhao, W.J.; Gong, H.L.; Deng, J.X. Susceptibility Analysis of Precipitation-induced Landslide Disaster-pregnant Environmental Factors Based on the Certainty Factor Probability Model—Taking the Hilly Area in Sichuan as Example. *J. Catastrophol.* **2014**, *29*, 109–115.
17. Hen, X.; Ran, H.; Qi, S. Triggering factors susceptibility of earthquake-induced landslides in the 1976 Longling earthquake. *Acta Sci. Nat. Univ. Pekin.* **2009**, *1*, 7.
18. Rezaei, M.; Noori, Z.Y.; Barmaki, M.D. Land subsidence susceptibility mapping using analytical hierarchy process (AHP) and Certain Factor (CF) models at Neyshabur plain, Iran. *Geocarto Int.* **2020**, *37*, 1465–1481. [CrossRef]
19. Lin, W.; Yin, K.; Wang, N.; Xu, Y.; Guo, Z.; Li, Y. Landslide hazard assessment of rainfall-induced landslide based on the CF-SINMAP model: A case study from Wuling Mountain in Hunan Province, China. *Nat. Hazards* **2021**, *106*, 679–700. [CrossRef]
20. Mao, Z.; Zhang, J.; Zhong, J. Wang, J; Sensitivity analysis on factors influencing loess terrace landslide potential using certainty factor method. *Bull. Soil Water Conserv.* **2023**, *43*, 183–192, 340.
21. Xiang, L.; Cui, P.; Zhang, J.; Huang, D.; Fang, H.; Zhou, X. Triggering factors susceptibility of earthquake-induced collapses and landslides in Wenchuan Count. *Adv. Eng. Sci.* **2010**, *42*, 105–112.
22. Liu, Y.; Chen, X.; Li, Q.; Yang, J.; Li, L.; Wang, T. Impact of different microphysics and cumulus parameterizations in WRF for heavy rainfall simulations in the central segment of the Tianshan Mountains, China. *Atmos. Res.* **2020**, *244*, 105052. [CrossRef]
23. Mock, C.J.; Kay, P.A. *Avalanche Climatology of the Western United States, with an Emphasis on Alta, Utah*; Blackwell Publishing Ltd.: Oxford, UK, 1992; Volume 44, pp. 307–318.
24. Hao, J.S.; Huang, F.R.; Liu, Y.; Amobichukwu, C.A.; Li, L.H. Avalanche activity and characteristics of its triggering factors in the western Tianshan Mountains, China. *J. Mt. Sci.* **2018**, *15*, 1397–1411. [CrossRef]
25. Föhn, P.; Stoffel, M.; Bartelt, P. Formation and Forecasting of Large (Catastrophic) New Snow Avalanches. In *Proceedings of the 2002 International Snow Science Workshop*; International Snow Science Workshop Canada: Whistler, BC, Canada, 2002.
26. Lobkina, V.A.; Gensiorovskiy, Y.V.; Muzychenko, A.A. Avalanche Hazard Assessment in Low Mountains, Based on the Example of the January 2021 Norilsk Avalanche Disaster. *Dokl. Earth Sci.* **2021**, *498*, 509–513. [CrossRef]
27. Liu, Y.; Li, L.H.; Chen, X.; Yang, J.M.; Hao, J.S. Spatial distribution of snow depth based on geographically weighted regression kriging in the Bayanbulak Basin of the Tianshan Mountains, China. *J. Mt. Sci.* **2018**, *15*, 33–45. [CrossRef]

28. Jomelli, V.; Delval, C.; Grancher, D.; Escande, S.; Brunstein, D.; Hetu, B.; Filion, L.; Pech, P. Probabilistic analysis of recent snow avalanche activity and weather in the French Alps. *Cold Reg. Sci. Technol.* **2007**, *47*, 180–192. [CrossRef]
29. Shortliffe, E.H.; Buchanan, B.G. A model of inexact reasoning in medicine. *Math. Biosci.* **1987**, *23*, 351–379. [CrossRef]
30. Heckerman, D. Probabilistic Interpretations for MYCIN's Certainty Factors. *Mach. Intell. Pattern Recognit.* **2013**, *4*, 167–196.
31. Hu, R.; Ma, W.; Wang, C. Investigation and analysis of snow Avalanches disaster in Western Tianshan Mountains of China. *J. Glaciol. Geocryol.* **1987**, *13–24*, 150.
32. Hu, R.; Chi, G.; Ma, W.; Cai, G. Research on avalanche control in the western Tianshan Mountains. *Xinjiang Geogr.* **1981**, *1*, 39–46.
33. Blagovecsenskii, V.-P.; Hu, R.G.; Ma, H. Avalanches and management of the Great Almajinka River Basin. *Arid. Zone Geogr.* **1994**, *17*, 11.
34. Qiu, J. *Avalanche Science*; Xinjiang Science and Technology Press: Urumqi, China, 2004.
35. Horton, S.; Towell, M.; Haegeli, P. Examining the operational use of avalanche problems with decision trees and model-generated weather and snowpack variables. *Copernic. Gmbh* **2020**, *20*, 3551–3576. [CrossRef]
36. Conway, H.; Wilbour, C. Evolution of snow slope stability during storms. *Cold Reg. Sci. Technol.* **1999**, *30*, 67–77. [CrossRef]
37. Hao, J.; Cui, P.; Zhang, X.; Li, L. Mechanisms of different types of avalanches induced by continental snow climate in the central Tianshan Mountains. *Sci. China Earth Sci.* **2022**, *52*, 2428–2440.
38. Lehning, S.M. Influence of snow cover properties on avalanche dynamics. *Cold Reg. Sci. Technol.* **2014**, *97*, 121–131.
39. Feick, S.; Kronholm, K.; Schweizer, J. Field observations on spatial variability of surface hoar at the basin scale. *J. Geophys. Res. Earth Surf.* **2007**, *112*. [CrossRef]
40. Hao, J.; Zhang, Z.; Li, L. Timing and identification of potential snow avalanche types: A case study of the central Tianshan Mountains. *Landslides* **2021**, *18*, 3845–3856. [CrossRef]
41. Maggioni, M.; Freppaz, M.; Christen, M.; Bartelt, P.; Zanini, E. Back-Calculation of Small Avalanches with the 2D Avalanche Dynamics Model Ramms: Four Events Artificially Triggered at the Seehore Test Site in Aosta Valley (NW Italy). In Proceedings of the 2012 International Snow Science Workshop, Anchorage, Alaska, 16–21 September 2012.
42. Zhou, J.; Fan, Q.; Zhu, Z. Analysis of driving factors of the geological disaster of debris flow in Guangxi based on the detector. *Geomat. Spat. Inf. Technol.* **2022**, *45*, 245–248.
43. Jamieson, B.; Johnston, C.D. Snowpack factors associated with strength changes of buried surface hoar layers. *Cold Reg. Sci. Technol.* **1999**, *30*, 19–34. [CrossRef]